Preprints of the 19th World Congress
The International Federation of Automatic Control
Cape Town, South Africa. August 24-29, 2014

Comparison of Nonlinear Flatness-Based Control of two Coupled Hydraulic Servo Cylinders

Robert Prabel * **Harald Aschemann** *

* *Chair of Mechatronics, University of Rostock, 18059 Germany (e-mail: {Robert.Prabel,Harald.Aschemann}@uni-rostock.de).*

Abstract:
This paper presents two nonlinear model-based control designs for a hydraulic system that consists of two mechanically coupled hydraulic cylinders actuated each by a separate servo-valve. Based on a physically-oriented nonlinear mathematical model of the test rig, a further model simplification results in a completely controllable MIMO system. Two different control structures are discussed and compared to each other in this paper: First, a cascaded flatness-based control is designed, where fast inner control loops determine the difference pressure in each hydraulic cylinder, while the position as well as the generated force is controlled in the outer loop. In the second approach, a centralised flatness-based control, with the same outputs as in the outer loop of the cascaded approach, is developed for the MIMO system. Model parameter uncertainties are estimated by a reduced-order disturbance observer and compensated by the control algorithm. The efficiency of the proposed control structures is demonstrated by experimental results from a dedicated test rig.

Keywords: nonlinear control, disturbance observer, hydraulic, flatness-based control, hydraulic cylinder, mechatronic system

1. INTRODUCTION

Nonlinear control for hydraulic systems becomes more and more attractive for highly dynamic positioning tasks that are subject to a variable load. A typical application is a hydraulic steer-by-wire system, see Haggag et al. (2005). In Sirouspour and Salcudean (2000) and in Sohl and Bobrow (1999), nonlinear control approaches for position-controlled hydraulic cylinders with one servo-valve are presented. The papers of Nakkarat and Kuntanapreeda (2009) as well as Sun and Chiu (1999) address nonlinear concepts for force-controlled hydraulic cylinders. A backstepping control for the position as well as a generated force of a coupled hydraulic cylinder is described in Prabel and Aschemann (2014). Further applications of the proposed flatness-based control design were published for other mechatronic systems in Aschemann et al. (2011) and Butt et al. (2012).

A test rig dedicated for the development and validation of sophisticated control approaches for hydraulic cylinder systems is available at the Chair of Mechatronics at the University of Rostock, see Fig. 1. In this paper, two nonlinear control concepts as well as corresponding experimental results from the hardware-in-the-loop (HIL) test rig are presented. The HIL test rig combines two control tasks: hydraulic positioning and generation of a specified disturbance force.

The test rig consists of two rigidly coupled hydraulic cylinders, which are actuated each by a separate servo valve. To guarantee a high bandwidth at force generating, two hydraulic capacities are directly installed in front of the second servo valve to maintain a constant pump pressure. Furthermore, in each hydraulic chamber a pressure sensor is available, and the actual position of the first hydraulic cylinder is measured. Due to the rigid mechanical connection between the cylinders and a geometric adjustment of the middle positions of both pistons, a further sensor for the second servo cylinder is not necessary. In between both cylinders, an additional force sensor is integrated that allows for a force measurement.

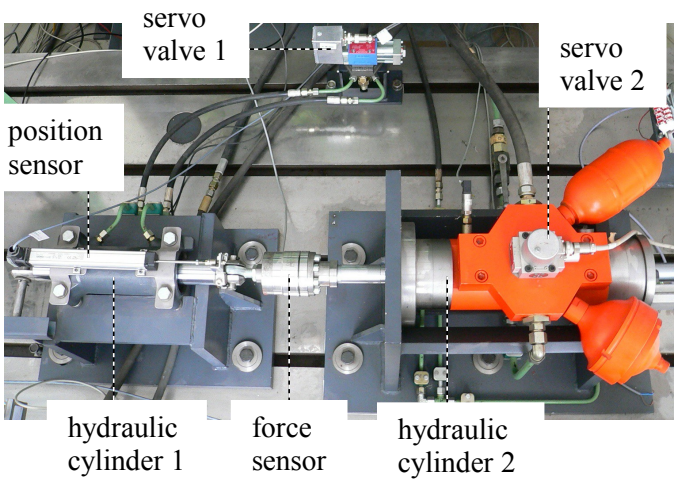

Fig. 1. Test rig for the hydraulic system.

The paper is structured as follows: First, a physically-oriented state-space model of the mechatronic system is derived and further simplified in subsequent model-order reduction step. Second, the differential flatness property is shown for the cascaded control as well as the centralised structure, and the corresponding control design is described. Third, a reduced-order disturbance observer is designed to estimate parameter uncertainties and disturbances like friction forces. Finally, experimental results show the advantages of the proposed control approaches

with only small tracking errors during transient phases as well as a negligible steady-state control error.

2. MODELLING OF THE MECHATRONIC SYSTEM

The mechatronic system can be split into a mechanical and a hydraulic subsystem. The mechanical system part covers the joint motion of the rigidly connected piston rods. The hydraulic subsystem describes the pressure dynamics in the cylinder chambers.

2.1 Mechanical Subsystem

The considered operation range of the system is characterized by values $-l_{max} < z(t) < l_{max}$, cf. Fig. 2. The equation of motion for the linked piston rods follows directly from a force balance. To differentiate between the two hydraulic cylinders, the index 1 is used for the left cylinder, whereas 2 denotes the right cylinder. The pressures $p_{1,A}(t)$ and $p_{1,B}(t)$ represent the two

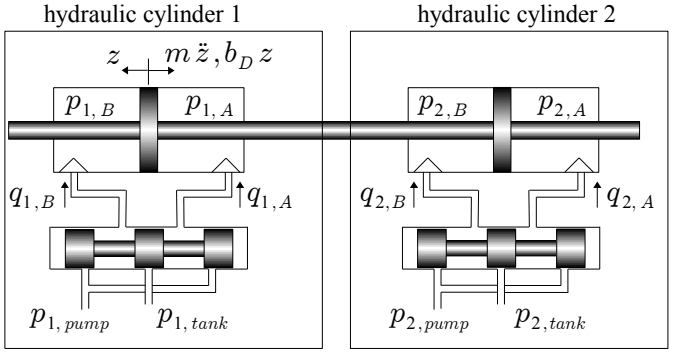

Fig. 2. Mechatronic model of the test rig.

absolute pressures in the right and left hydraulic chamber the first cylinder. The corresponding force on the piston is given by $F_1(t) = A_1\,(p_{1,A}(t) - p_{1,B}(t))$. Here, A_1 stands for the piston area of the first cylinder. For the second cylinder, the driving force is given by $F_2(t) = A_2\,(p_{2,A}(t) - p_{2,B}(t))$. The absolute pressures are denoted by $p_{2,A}(t)$ and $p_{2,B}(t)$, and A_2 stands for the piston area for the second cylinder. Furthermore, a velocity proportional damping force $F_D(t) = \dot{z}(t)\,b_D$ is considered in the model.

A balance of momentum yields the equation of motion in the form of a second order differential equation

$$\begin{aligned}\ddot{z}(t) = \frac{1}{m}\,[&-\dot{z}(t)\,b_D + A_1\,(p_{1,A}(t) - p_{1,B}(t)) \\ &+ A_2\,(p_{2,A}(t) - p_{2,B}(t)) - F_U(t)]\,,\end{aligned} \tag{1}$$

with m as the reduced mass of all the moving components connected to the hydraulic cylinders. Model uncertainty and nonlinear friction could be advantageously taken into account by a lumped disturbance force $F_U(t)$.

2.2 Hydraulic Subsystem

A mass flow balance for one of the four cylinder chambers, $i \in \{1,2\}$ and $j \in \{A,B\}$, directly leads to

$$\frac{dm_{i,j}(t)}{dt} = \dot{\rho}_{i,j}(t) \cdot V_{i,j}(z(t)) + \rho_{i,j}(t) \cdot \dot{V}_{i,j}(\dot{z}(t)) = \rho_{i,j}(t)\,q_{i,j}(t). \tag{2}$$

Here, the density $\rho_{i,j}(t)$, the chamber volume $V_{i,j}(z(t))$ and the volume flow $q_{i,j}(t)$ into the corresponding cylinder chamber are introduced. The elastic model of the hydraulic fluid is defined as

$$dp_{i,j}(t) = -E(p_{i,j})\frac{dV_{i,j}}{V_{i,j}}, \tag{3}$$

with the bulk modulus $E(p_{i,j})$ of the hydraulic fluid, which in general depends on the pressure. In this paper, however, E can be assumed with high accuracy as constant in the given pressure range. Mass conservation leads to the relationship

$$-\frac{dV_{i,j}}{V_{i,j}} = \frac{d\rho_{i,j}}{\rho_{i,j}}. \tag{4}$$

This results in the pressure dynamics

$$\dot{p}_{i,j}(t) = -\frac{E\,\dot{V}_{i,j}(\dot{z})}{V_{i,j}(z)} + \frac{E}{V_{i,j}(z)}q_{i,j}(t)\,. \tag{5}$$

The differential equations for the pressures in the chambers j, $j \in \{A,B\}$, of cylinder i, $i \in \{1,2\}$, become

$$\begin{aligned}\dot{p}_{i,A}(t) &= -\frac{E\,A_i\,\dot{z}(t)}{V_{i,0} + A_i\,z(t)} + \frac{E}{V_{i,0} + A_i\,z(t)}q_{i,A}(t) \quad \text{and} \\ \dot{p}_{i,B}(t) &= \frac{E\,A_i\,\dot{z}(t)}{V_{i,0} - A_i\,z(t)} + \frac{E}{V_{i,0} - A_i\,z(t)}q_{i,B}(t).\end{aligned} \tag{6}$$

Here, the volume chambers are characterized by $V_{i,A} = V_{i,0} + A_i\,z(t)$ and $V_{i,B} = V_{i,0} - A_i\,z(t)$, and the volume flows $q_{i,A}(t)$ and $q_{i,B}(t)$ serve as control inputs.

2.3 Model-Order Reduction and Derivation of Decentralised Models

An overall nonlinear state-space model for the whole test rig in the form $\dot{\underline{x}} = \underline{f}(\underline{x},\underline{u})$ can be stated as

$$\dot{\underline{x}} = \begin{bmatrix} \dot{z} \\ \frac{1}{m}\,[-\dot{z}\,b_D + A_1\,(p_{1,A} - p_{1,B}) + A_2\,(p_{2,A} - p_{2,B}) - F_U] \\ -\frac{E\,A_1\,\dot{z}}{V_{1,0} + A_1\,z} + \frac{E}{V_{1,0} + A_1\,z}q_{1,A} \\ \frac{E\,A_1\,\dot{z}}{V_{1,0} - A_1\,z} + \frac{E}{V_{1,0} - A_1\,z}q_{1,B} \\ -\frac{E\,A_2\,\dot{z}}{V_{2,0} + A_2\,z} + \frac{E}{V_{2,0} + A_2\,z}q_{2,A} \\ \frac{E\,A_2\,\dot{z}}{V_{2,0} - A_2\,z} + \frac{E}{V_{2,0} - A_2\,z}q_{2,B} \end{bmatrix}, \tag{7}$$

with the state vector $\underline{x} = [z\ \dot{z}\ p_{1,A}\ p_{1,B}\ p_{2,A}\ p_{2,B}]^T$, the input vector $\underline{u} = [q_{1,A}\ q_{1,B}\ q_{2,A}\ q_{2,B}]^T$ and the output vector $\underline{y} = [z\ ((p_{1,A} - p_{1,B}) \cdot A_1 - (p_{2,A} - p_{2,B}) \cdot A_2)/2]^T$. This nonlinear model, however, turns out to be not completely controllable.

In the following, a model-order reduction is performed. For this purpose, a new state variable in form of the difference pressure $\Delta p_i(t) = p_{i,A}(t) - p_{i,B}(t)$ is introduced, where $i \in \{1,2\}$ indicates the individual cylinder. The corresponding differential equation can be stated as

$$\begin{aligned}\Delta\dot{p}_i(t) &= \dot{p}_{i,A}(t) - \dot{p}_{i,B}(t) \\ &= -\frac{E\,A_i\,\dot{z}}{V_{i,A}(z)} + \frac{E}{V_{i,A}(z)}\,q_{i,A}(t) - \frac{E\,A_i\,\dot{z}}{V_{i,B}(z)} - \frac{E}{V_{i,B}(z)}\,q_{i,B}(t).\end{aligned} \tag{8}$$

Furthermore, the relationship between the volume flow into chamber A and out of chamber B is given by $q_{i,A}(t) = -q_{i,B}(t)$. Thereby the effective volume flow for the difference pressure is defined as $q_{i,AB}(t) = q_{i,A}(t) - q_{i,B}(t) = 2\,q_{i,A}(t)$. The product of

the volumes can be written as $V_{i,A}(z) \cdot V_{i,B}(z) = V_{i,0}^2 - (A_i \cdot z)^2$, and the sum becomes $V_{i,A}(z) + V_{i,B}(z) = 2 \cdot V_{i,0}$, with $V_{i,A}(z) = V_{i,0} + A_i z$ and $V_{i,B}(z) = V_{i,0} - A_i z$. The resulting differential equation for the difference pressure dynamics is

$$\Delta\dot{p}_i(t) = \frac{-2EA_iV_{i,0}\dot{z}}{V_{i,0}^2 - (A_i \cdot z)^2} + \frac{EV_{i,0}}{V_{i,0}^2 - (A_i \cdot z)^2} q_{i,AB}(t) . \quad (9)$$

Note that this formulation for the difference pressure dynamics holds for both hydraulic cylinders. Thereby, the dimension of the state vector is reduced from $dim(\underline{x}) = 6$ to $dim(\underline{x}_r) = 4$. The dynamics of the MIMO system is described by

$$\dot{\underline{x}}_r = \begin{bmatrix} \dot{z} \\ \frac{-b\dot{z}}{m} + \frac{A_1\Delta p_1(t)}{m} + \frac{A_2\Delta p_2(t)}{m} - \frac{F_U}{m} \\ \frac{-2EA_1V_{1,0}\dot{z}}{V_{1,0}^2 - (A_1 \cdot z)^2} + \frac{EV_{1,0}}{V_{1,0}^2 - (A_1 \cdot z)^2} q_{1,AB}(t) \\ \frac{-2EA_2V_{2,0}\dot{z}}{V_{2,0}^2 - (A_2 \cdot z)^2} + \frac{EV_{2,0}}{V_{2,0}^2 - (A_2 \cdot z)^2} q_{2,AB}(t) \end{bmatrix} . \quad (10)$$

The position $z(t)$ and force $F(t) = (A_1\Delta p_1(t) - A_2\Delta p_2(t))/2$ are considered as outputs. The corresponding input vector is given by $\underline{u}(t) = [q_{1,AB}(t)\ q_{2,AB}(t)]$ and the state vector is chosen as $\underline{x}_r(t) = [z(t)\ \dot{z}(t)\ \Delta p_1(t)\ \Delta p_2(t)]$.

2.4 Valve Characteristic

The volume flow through a hydraulic valve is usually modelled as an ideal turbulent resistance with variable cross-section. At the given test rig, the two valves have an analogue voltage signal as input, respectively. The volume flow through a hydraulic resistance with variable cross-section area is given by

$$q_i = B_{i,V} \cdot u_i \cdot \sqrt{\Delta p_V} , \quad (11)$$

with $B_{i,V}$ as the valve conductance, u_i the valve input signal and Δp_V the pressure difference between the pressure in front of and behind the valve.

Instead of using the mathematical description of the volume flow (11), both valve characteristics are experimentally identified at the test rig shown in Fig. 1.

The identified valve characteristics for the first cylinder, for example, is depicted in Fig. 3(a). It can be inverted, see Fig. 3(b), in such a way that the analogue voltage signal for the valve is determined by the actual valve difference pressure Δp_V and the volume flow $q_{i,AB}$. The inverted valve characteristics are employed in the control structures depicted in Fig. 4 and Fig. 5.

3. FLATNESS-BASED CONTROL DESIGN

A nonlinear system – usually given in the form $\dot{\underline{x}} = \underline{f}(\underline{x}, \underline{u})$ – is denoted as differential flat, see M. Fliess, J. Levine, P. Martin and P. Rouchon (1995), if appropriate flat outputs $\underline{y} = \underline{y}(\underline{x}, \underline{u}, \dot{\underline{u}}, ..., \underline{u}^l)$ exist that:

(i) allow for expressing all system states $\underline{x}$ and all system inputs $\underline{u}$ as a function of these flat outputs $\underline{y}$ as well as their time derivatives, i.e. $\underline{x} = \underline{x}\left(\underline{y}, \dot{\underline{y}}, \ldots, \underline{y}^{(\beta)}\right)$ and $\underline{u} = \underline{u}\left(\underline{y}, \dot{\underline{y}}, \ldots, \underline{y}^{(\beta+1)}\right)$,
(ii) are differentially independent, i.e., they are not connected by differential equations.

If the first condition is fulfilled, the second condition is equivalent to $\dim\left(\underline{y}\right) = \dim\left(\underline{u}\right)$. In this paper, both a cascaded and a centralised control approach are considered. In the case of the cascaded control approach, fast inner control loops are designed for the difference pressures Δp_i as flat outputs. Moreover, the position z as well as the generated force F represent the flat outputs of the outer control loop. Following the centralised approach, a MIMO control for the position z as well as the generated force F is developed.

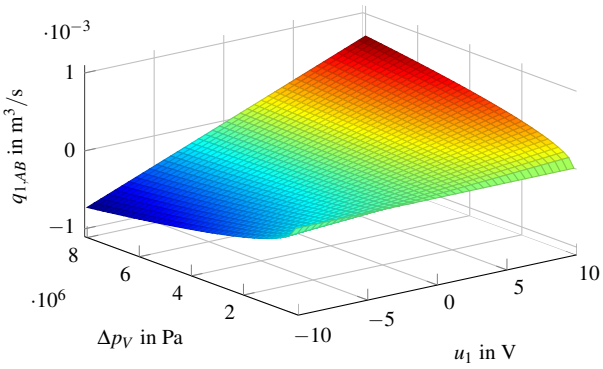

(a) Identified volume flow characteristic of the valve for the first cylinder

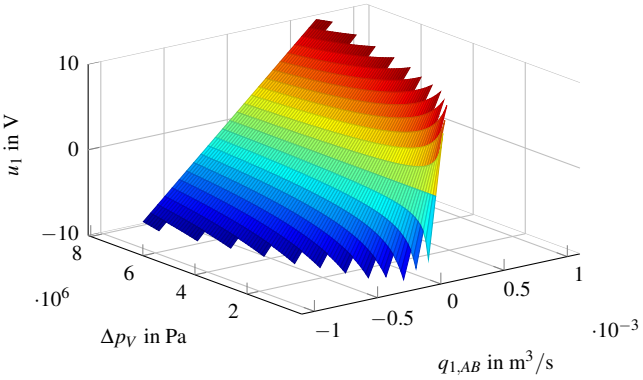

(b) Inverted volume flow characteristic of the valve for the first cylinder

Fig. 3. Identified and inverted volume flow characteristics.

3.1 Inner control loops for the difference pressures of the hydraulic cylinders

In both hydraulic subsystems, the first time derivative of the flat output candidate $y_{f,p}(t) = \Delta p_i(t)$ becomes

$$\Delta\dot{p}_i(t) = \frac{-2EA_iV_{i,0}\dot{z}}{V_{i,0}^2 - (A_i \cdot z)^2} + \frac{EV_{i,0}}{V_{i,0}^2 - (A_i \cdot z)^2} q_{i,AB}(t) . \quad (12)$$

As it is affected by the control input, equation (12) can be solved for the input variable $q_{i,AB}(t)$. This results in the following inverse model depending on the flat output and its first time derivative

$$q_{i,AB}(t) = \frac{\nu_{\Delta p,i}(t) \cdot (V_{i,0}^2 - (A_i \cdot z(t))^2)}{EV_{i,0}} + 2A_i\dot{z}(t) , \quad (13)$$

with $\nu_{\Delta p,i} = \Delta\dot{p}_i$ as the stabilising control input. For these flat outputs, the stabilising control input is chosen as

$$\nu_{\Delta p,i} = \Delta\dot{p}_{i,d} + \alpha_{\Delta p,i}\left(p_{i,d} - p_i\right) . \quad (14)$$

3.2 Outer control loop for the cylinder position and the generated force

The mechanical system part also represents a differentially flat system, with the position $z(t)$ of the first hydraulic cylinder

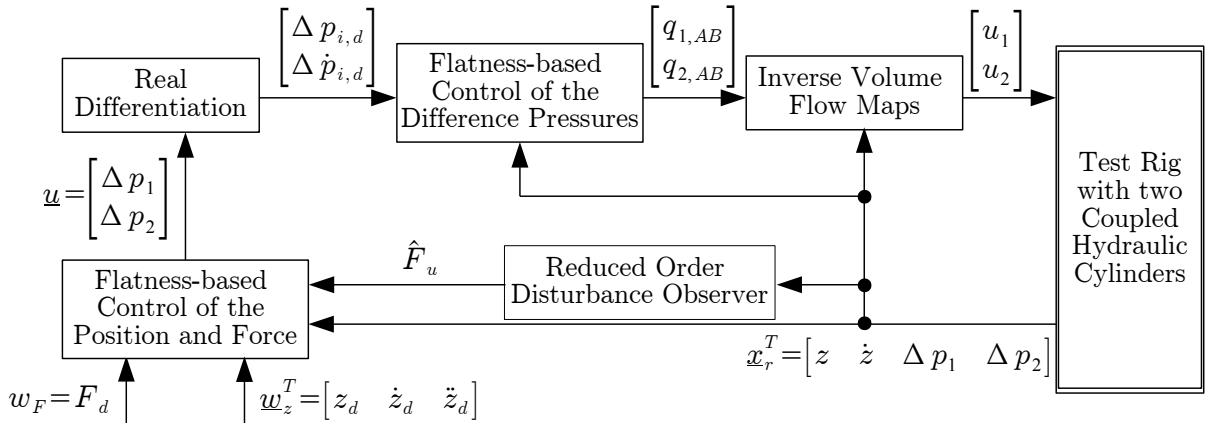

Fig. 4. Implementation of the cascaded flatness-based control.

and the force $F(t) = (A_1\,\Delta p_1(t) - A_2\,\Delta p_2(t))/2$ as flat outputs. Subsequent differentiations of the first flat output $y_1(t) = z(t)$, until one of the control inputs $(\Delta p_1(t),\ \Delta p_2(t))$ appears, leads to

$$\begin{aligned} y_1 &= z\,,\ \dot{y}_1 = \dot{z}\,,\\ \ddot{y}_1 &= \ddot{z}(t) = \frac{1}{m}\left[-\dot{z}(t)\,b_D + A_1\,\Delta p_1 + A_2\,\Delta p_2 - F_U(t)\right], \end{aligned} \tag{15}$$

whereas the second variable directly depends on the control inputs

$$y_2(t) = F(t) = (A_1\,\Delta p_1(t) - A_2\,\Delta p_2(t))/2\,. \tag{16}$$

The inverse dynamics can be obtained by solving the equations (15) and (16) for the input variables $\Delta p_1(t)$ and $\Delta p_2(t)$. Hence, the input vector $\underline{u}(t)$ depending on the desired force F and the control input $v_z = \ddot{z}$ is given by

$$\underline{u}(t) = \begin{bmatrix}\Delta p_1(t)\\ \Delta p_2(t)\end{bmatrix} = \begin{bmatrix}\frac{1}{2A_1}(m\cdot v_z + 2F + b\,\dot{z} + F_U)\\ \frac{1}{2A_2}(m\cdot v_z - 2F + b\,\dot{z} + F_U)\end{bmatrix}. \tag{17}$$

The stabilising control input v_z for the position error is chosen as

$$v_z = \ddot{z}_d + \alpha_{z,1}\,(\dot{z}_d - \dot{z}) + \alpha_{z,0}\,(z_d - z)\,. \tag{18}$$

The coefficients $\alpha_{z,k}$, $k \in \{0,1\}$, are specified in such a way as to obtain an asymptotically stable error dynamics with small tracking errors. The implementation of the cascaded control structure is shown in Fig. 4.

3.3 Centralised flatness-based control for the cylinder position and the force between the coupled cylinders

To design a centralised flatness-based control, the reduced-order model (10) with the input variables $q_{i,AB}$ is used. The time derivatives of the first flat output result in

$$\begin{aligned} y_1 &= z\,,\ \dot{y}_1 = \dot{z}\,,\\ \ddot{y}_1 &= \ddot{z}(t) = \frac{1}{m}\left[-\dot{z}(t)\,b_D + A_1\,\Delta p_1 + A_2\,\Delta p_2 - F_U(t)\right],\\ \dddot{y}_1 &= \dddot{z}(t) = \frac{1}{m}\left[-\ddot{z}(t)\,b_D + A_1\,\Delta \dot{p}_1 + A_2\,\Delta \dot{p}_2 - \dot{F}_U(t)\right],\\ &= g_1(z,\dot{z},\Delta p_1,\Delta p_2,q_{1,AB},q_{2,AB},F_U,\dot{F}_U)\,. \end{aligned} \tag{19}$$

In (19), the third time derivative is affected by the control inputs. The following equations

$$\begin{aligned} y_2(t) &= F(t) = (A_1\,\Delta p_1(t) - A_2\,\Delta p_2(t))/2\,,\\ \dot{y}_2(t) &= \dot{F}(t) = (A_1\,\Delta \dot{p}_1(t) - A_2\,\Delta \dot{p}_2(t))/2\,,\\ &= g_2(z,\dot{z},\Delta p_1,\Delta p_2,q_{1,AB},q_{2,AB})\,. \end{aligned} \tag{20}$$

show that the first time derivative of the second flat output y_2 is influenced by the control inputs. The inverse dynamics of the centralised control structure is calculated by solving $v_1 = g_1$ and $v_2 = g_2$ for the control inputs $q_{i,AB}$. The corresponding stabilisation of the error dynamics is achieved with

$$\begin{aligned} v_1 &= \dddot{z}_d + \beta_{z,2}\,(\ddot{z}_d - \ddot{z}) + \beta_{z,1}\,(\dot{z}_d - \dot{z}) + \beta_{z,0}\,(z_d - z)\,,\\ v_2 &= \dot{F}_d + \beta_{F,0}\,(F_d - F)\,. \end{aligned} \tag{21}$$

As before, the coefficients $\beta_{z,\phi}$, $\phi \in \{0,1,2\}$, and $\beta_{F,0}$ are chosen as coefficients of Hurwitz polynomials. In Fig. 5, the implementation of the centralised control structure is shown.

3.4 Reduced-order disturbance observer

To consider model uncertainties, e.g. friction and unknown parameters, represented by the lumped disturbance force F_U in the control strategy, a reduced-order disturbance observer according to Friedland (1996) is introduced. The key idea for the observer design is to extend the state equations with an integrator as disturbance model

$$\dot{\underline{y}} = \underline{f}(\underline{y},F_U,u)\,,\ \ \dot{F}_U = 0\,, \tag{22}$$

where $\underline{y} = \underline{x}_r$ represents the fully measurable state vector. The lumped disturbance force $\hat{F}_U$ to be estimated is obtained from

$$\hat{F}_U = \underline{h}^T\cdot\underline{y} + \xi\,, \tag{23}$$

with the observer gain vector $\underline{h}^T = [\,0\ h_2\ 0\ 0\,]$. The state equation for ξ is given by

$$\begin{aligned} \dot{\xi} &= \Phi\left(\underline{y},\hat{F}_U,u\right)\\ &= -h_2\cdot\left(1/m\cdot(\Delta p_1 A_1 + \Delta p_2 A_2 - b\,\dot{z} - \hat{F}_U)\right). \end{aligned} \tag{24}$$

The observer gain vector $\underline{h} = [0,h_2]^T$ and the function Φ have to be chosen properly, so that the steady-state observer error $e = F_U - \hat{F}_U$ converges to zero. Thus, the function Φ can be determined as follows

$$\dot{e} = 0 = \dot{F}_U - \underline{h}^T\cdot\dot{\underline{y}} - \Phi\left(\underline{y},F_U - 0,u\right)\,. \tag{25}$$

In view of $\dot{F}_U = 0$, equation (25) leads to

$$\Phi\left(\underline{y},F_U,u\right) = -\underline{h}^T\cdot\underline{f}(\underline{y},F_U,u)\,. \tag{26}$$

The linearized error dynamics must be asymptotically stable. Accordingly, the eigenvalue of the scalar Jacobian

$$J_e = \frac{\partial\Phi\left(\underline{y},F_U,u\right)}{\partial F_U} = -h_2\cdot\frac{1}{m}, \tag{27}$$

is placed in the left complex half-plane. This can be achieved by a proper choice of the scalar observer gain h_2. The stability

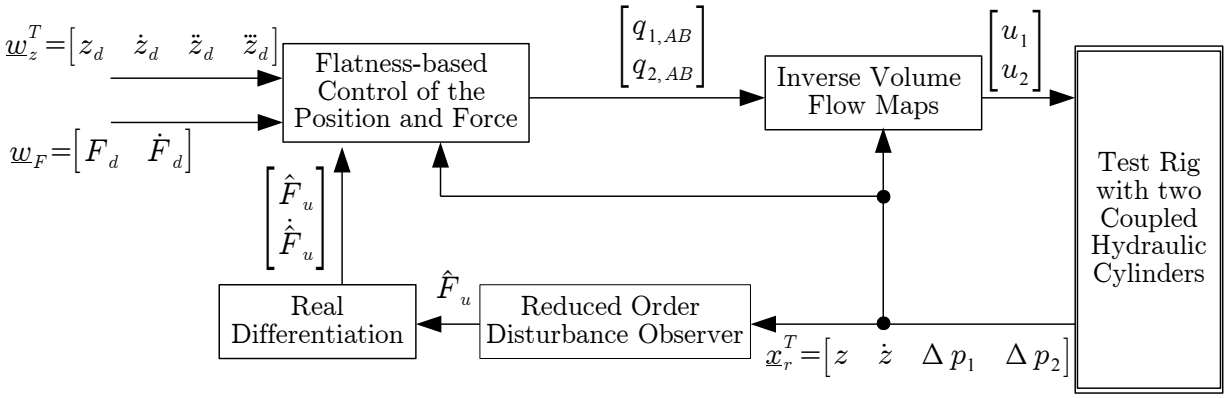

Fig. 5. Implementation of the centralised flatness-based control.

of the closed-loop control system has been investigated by simulations.

4. EXPERIMENTAL RESULTS

In the following, experimental results for the coupled hydraulic cylinders are presented to point out the benefits using the flatness-based control approach. Each electro-hydraulic valve is connected to a separate hydraulic pump, with a supply pressure of $p_{1,pump} = p_{2,pump} = 80 \cdot 10^5$ Pa. The desired trajectories

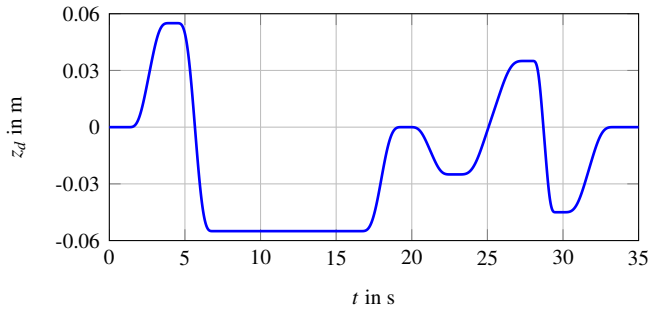

Fig. 6. Desired trajectory for the position of the coupled cylinders.

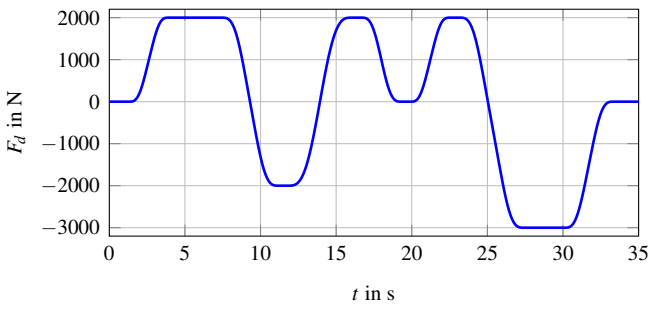

Fig. 7. Desired trajectory for the force of the coupled cylinders.

for the position and the force are depicted in Fig. 6 and 7, respectively.

In the following, the tracking errors of the four flatness-based control structures are compared to each other: 1) cascaded (CC), 2) cascaded with observer (CCO), 3) centralised (CE), and 4) centralised with observer (CEO).

Fig. 8 and Fig. 9 shows the obtained tracking errors for the four approaches: Obviously, the smallest position tracking errors of mostly below 0.1 mm can be obtained with the CCO structure. Without a disturbance observer, the position errors using CC are slightly larger. The force tracking errors of the cascaded approaches are very similar to each other, see Fig. 8b and Fig. 8c. This is a result of the disturbance observer, which affects only the position tracking part. The centralised control approach leads to tracking errors that are 10 times larger as those of the cascaded one. Regarding the force tracking errors, however, the difference between the cascaded and the centralised structure is negligible.

Furthermore, the force tracking errors in the transient phases of the position trajectory stem from the real differentiation of the measured position signal, which is employed in the inner control loops for the difference pressures of the hydraulic cylinders. Measurement noise of the four pressure sensors is reflected in the force tracking errors shown in Fig. 8b and Fig. 9b.

The corresponding root-mean square errors for the position and the generated force

$$e_{RMS,i} = \sqrt{\frac{1}{N}\sum_{k=1}^{N} e_i^2(k)}$$

with $i \in \{z, F\}$ are shown for all the investigated control structures in table 1.

	CC	CCO	CE	CEO
$e_{RMS,z}$	0.052 mm	0.027 mm	0.59 mm	0.54 mm
$e_{RMS,F}$	71 N	64 N	65 N	69 N

Table 1. Root mean square errors of the cylinder position and the generated force

5. CONCLUSIONS

In this paper, a cascaded and a centralised flatness-based control design are employed for a hydraulic system that consists of two coupled hydraulic cylinders. Based on a control-orientated model of the system, a model-order reduction is performed that leads to a completely controllable state-space representation. A reduced-order disturbance observer is estimating a lumped

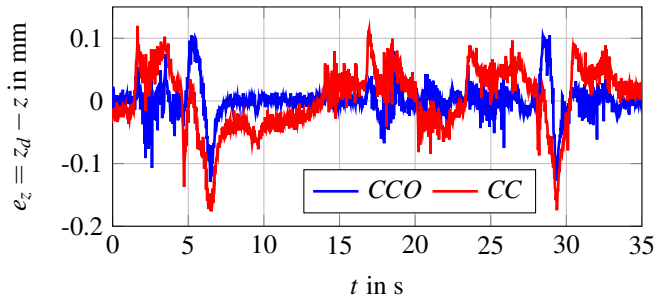

(a) Position tracking error

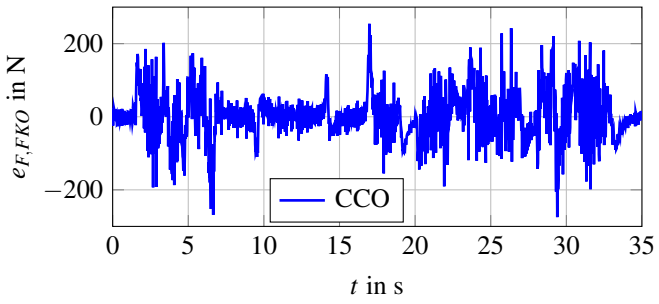

(b) Force tracking error

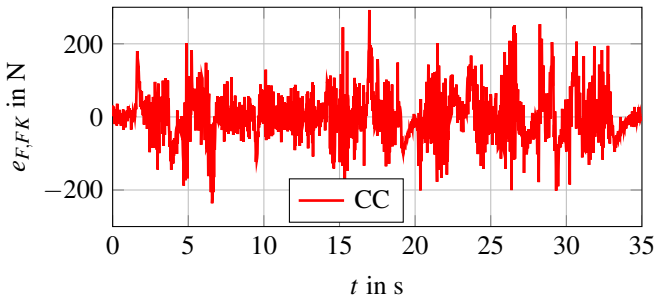

(c) Force tracking error

Fig. 8. Experimental results using the cascaded structures CCO and CC.

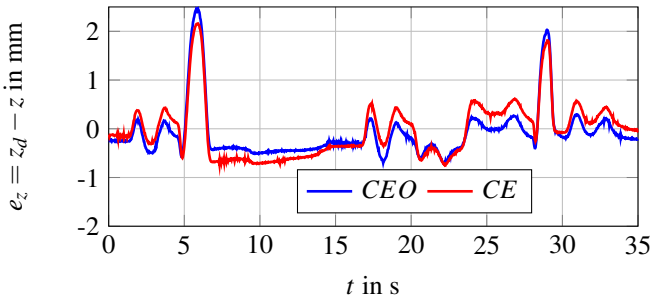

(a) Position tracking error

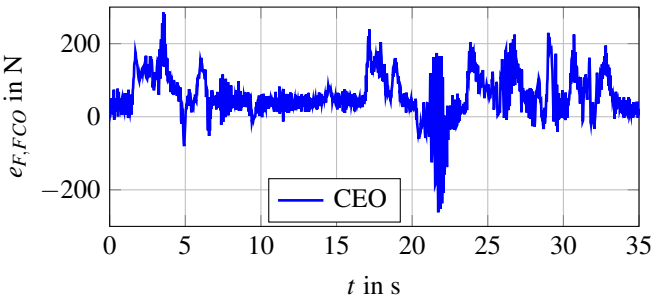

(b) Force tracking error

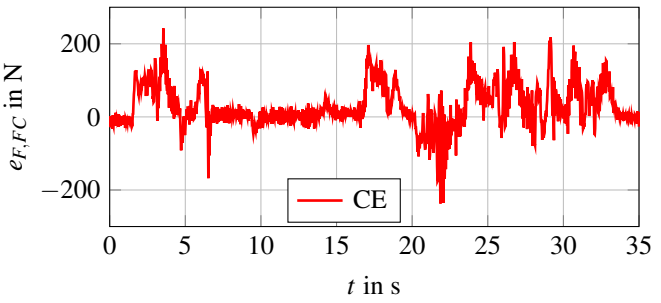

(c) Force tracking error

Fig. 9. Experimental results using the centralised structures CEO and CE.

disturbance force accounting for parameter uncertainties and nonlinear friction. The control performance and the efficiency of the proposed control structures are pointed out by experimental results from an implementation on a dedicated test rig at the Chair of Mechatronics, University of Rostock. The obtained maximum tracking errors for the CCO structure are approx. $e_z = 0.1$ mm for the cylinder position and approx. $e_F = 220$ N for the force.

REFERENCES

Aschemann, H., Prabel, R., Gross, C., and Schindele, D. (2011). Flatness-based control for an internal combustion engine cooling system. In *Proceedings of the 2011 IEEE International Conference on Mechatronics (ICM)*, 140–145. doi: 10.1109/ICMECH.2011.5971271.

Butt, S., Prabel, R., and Aschemann, H. (2012). Flatness-based control and observer design scheme for hybrid synchronous machines. In *Proceedings of the 2012 7th IEEE Conference on Industrial Electronics and Applications (ICIEA)*, 925–930. doi:10.1109/ICIEA.2012.6360856.

Friedland, B. (1996). *Advanced Control System Design*. Prentice-Hall.

Haggag, S., Alstrom, D., Cetinkunt, S., and Egelja, A. (2005). Modeling, control, and validation of an electro-hydraulic steer-by-wire system for articulated vehicle applications. *Mechatronics, IEEE/ASME Transactions on*, 10(6), 688–692. doi:10.1109/TMECH.2005.859838.

M. Fliess, J. Levine, P. Martin and P. Rouchon (1995). Flatness and defect of nonlinear systems: Introductory theory and examples. *Int. J. Control*, 61, 1327–1361.

Nakkarat, P. and Kuntanapreeda, S. (2009). Observer-based backstepping force control of an electrohydraulic actuator. *Control Engineering Practice*, 17(8), 895–902.

Prabel, R. and Aschemann, H. (2014). Nonlinear adaptive backstepping control of two coupled hydraulic servo cylinders. In *Proceedings of the 2014 American Control Conference (ACC)*.

Sirouspour, M.R. and Salcudean, S. (2000). On the nonlinear control of hydraulic servo-systems. In *Proceedings of IEEE International Conference on Robotics and Automation, (ICRA), San Francisco, USA*, volume 2, 1276–1282.

Sohl, G.A. and Bobrow, J.E. (1999). Experiments and simulations on the nonlinear control of a hydraulic servosystem. *IEEE Transactions on Control Systems Technology*, 7(2), 238–247.

Sun, H. and Chiu, G.C. (1999). Nonlinear observer based force control of electro-hydraulic actuators. In *Proceedings of the 1999 American Control Conference, (ACC), San Diego, USA*, volume 2, 764–768.